ISSN 0915-633X

INTERNATIONAL ATOMIC ENERGY AGENCY

SIXTEENTH IAEA FUSION ENERGY CONFERENCE

Montréal, Canada, 7-11 October 1996

IAEA-CN-64/C1-2

NATIONAL INSTITUTE FOR FUSION SCIENCE

Edge Plasma Control by a Local Island Divertor in the Compact Helical System

A. Komori, N. Ohyabu, S. Masuzaki, T. Morisaki, H. Suzuki, C. Takahashi, S. Sakakibara, K. Watanabe, T. Watanabe, T. Minami, S. Morita, K. Tanaka, S. Ohdachi, S. Kubo, N. Inoue, H. Yamada, K. Nishimura, S. Okamura, K. Matsuoka, O. Motojima, M. Fujiwara, A. Iiyoshi, C. C. Klepper, J.F. Lyon, A.C. England, D.E. Greenwood, D.K. Lee, D.R. Overbey, J.A. Rome, D.E. Schechter and C.T. Wilson

(Received - Aug. 19, 1996)

NIFS-438 Sep. 1996

RESEARCH REPORT
NIFS Series

NAGOYA, JAPAN

INTERNATIONAL ATOMIC ENERGY AGENCY

SIXTEENTH IAEA FUSION ENERGY CONFERENCE

Montréal, Canada, 7–11 October 1996

IAEA-CN-64/C1-2

EDGE PLASMA CONTROL BY A LOCAL ISLAND DIVERTOR IN THE COMPACT HELICAL SYSTEM

A. KOMORI, N. OHYABU, S. MASUZAKI, T. MORISAKI, H. SUZUKI, C. TAKAHASHI, S. SAKAKIBARA, K. WATANABE, T. WATANABE, T. MINAMI, S. MORITA, K. TANAKA, S. OHDACHI, S. KUBO, N. INOUE, H. YAMADA, K. NISHIMURA, S. OKAMURA, K. MATSUOKA, O. MOTOJIMA, M. FUJIWARA and A. IIYOSHI

National Institute for Fusion Science, Nagoya 464-01, Japan

C. C. KLEPPER, J. F. LYON, A. C. ENGLAND, D. E. GREENWOOD, D. K. LEE, D. R. OVERBEY, J. A. ROME, D. E. SCHECHTER and C. T. WILSON

Oak Ridge National Laboratory, Oak Ridge, TN 37831-8072, USA

EDGE PLASMA CONTROL BY A LOCAL ISLAND DIVERTOR IN THE COMPACT HELICAL SYSTEM

ABSTRACT

A local island divertor (LID) experiment was performed on the Compact Helical System (CHS) to demonstrate the principle of the LID. It was clearly demonstrated that the particle flow is controlled by adding a resonant perturbation field to the CHS magnetic configuration, and guided to the back side of an m/n=1/1 island which is created by the perturbation field. The particles recycled there were pumped out with a pumping rate in the range from a few percent to about 10%. As a result, the line-averaged core density was reduced compared with non-LID discharges at the same gas puff rate by a factor of about 2. In addition to the demonstration of these fundamental divertor functions, a modest improvement of energy confinement was observed, which could be attributed to the edge plasma control by the LID.

1. INTRODUCTION

The Large Helical Device (LHD) is a superconducting heliotron-type device under construction at the National Institute for Fusion Science at Toki, Japan [1]. One of the key research issues in the LHD program is to enhance helical plasma performance through the edge plasma control. The edge plasma behavior is important in determining heat and particle fluxes to the wall and enhancing core plasma confinement. This control of the LHD edge plasma will primarily be done with a closed full helical divertor which utilizes a natural separatrix in the edge region [2]. However, the closed full helical divertor will not be ready in the early stage of the LHD experiment. Instead we plan to use a local island divertor (LID) for the LHD edge plasma control [3]. The LID is a closed divertor that uses an m/n=1/1 island. The technical ease of hydrogen pumping is the advantage of the LID over the closed full helical divertor because the hydrogen recycling is toroidally localized. The experimental study to demonstrate the principle of the LID was done in detail on the Compact Helical System (CHS) in Nagoya, Japan. The results obtained are described in this paper. The LID experiment on CHS has provided us critical information on the edge plasma behavior in the heliotron-type device, and helped us to optimize the design of the LID and the closed full helical divertor on LHD. It has also influenced the divertor design of the W7-AS [4] and the W7-X [4,5], and helped us to explore advanced divertor concepts.

2. EXPERIMENTAL APPARATUS

For the CHS experiment, a resonant perturbation field $\tilde{b}$ necessary for an m/n=1/1 island was generated by 16 small perturbation coils located above and below the CHS vacuum vessel. The outward heat and particle fluxes crossing the island separatrix flow along the field lines to the back side of the island, where carbon (or stainless steel) target plates of 10 mm (2 mm) in thickness are placed on a divertor head, as shown Fig. 1(a) [3]. Figure 1(b) shows a schema explaining the relation between the divertor head and island. The particles recycled there are pumped out by a cryogenic pump with a

hydrogen pumping speed of 21,000 lit./s. The divertor head consists of 18 small planar plates, although ideally they should be three-dimensional curved tiles which match the magnetic surface. The geometrical shapes of the divertor head and pumping duct are designed to form a closed divertor configuration with high pumping efficiency [3]. The gap between the divertor head and pumping duct was fixed at 4 cm in our experiment. For the standard LID configuration, the leading edges of the divertor head, i.e., those of the target plates are located well inside the island, thereby being protected from the outward heat flux from the core [3].

The CHS device was operated with a toroidal magnetic field B_0 of 0.9 T and a magnetic axis position R_{ax} of 99.5 cm [6]. The $\iota/2\pi=1$ flux surface is well inside the vacuum vessel wall when $R_{ax} > 97.4$ cm. The plasma was produced by ion Bernstein wave (IBW) and/or second-harmonic electron cyclotron heating (ECH) and was heated by 0.82 MW tangential neutral beam injection (NBI) at 38 keV. The following instruments were used as the key diagnostics systems of this experiment; an IR TV camera for surface temperature measurements, a CCD TV camera with an optical filter for Hα measurements, Langmuir probes for edge plasma measurements and an ASDEX style fast-ion gauge system [7] for measurements of the neutral hydrogen pressure in the pumping duct.

3. EXPERIMENTAL RESULTS AND DISCUSSION

The m/n=1/1 island geometry of the LID was confirmed by mapping the magnetic surfaces. The mapping was carried out by the fluorescent method, using an electron gun with a W filament and a fluorescent mesh which emits light if the electron beam collides with it. The arrangement of the mapping apparatus is shown in Fig. 2. The fluorescent mesh is situated at the same toroidal position as the divertor head. The magnetic surfaces were measured by taking pictures of the beam positions on the fluorescent mesh while changing the radial position of the electron gun. The mapping was performed in a steady-state operation at low field, B_0=0.0875 T, and a clear picture of

the m/n=1/1 island was obtained [8]. The island is located at the radial position that is predicted theoretically. However, the width of the island is a little wider than the expected value, and the island is not symmetrical with respect to the equatorial plane. This is because a "natural" m/n=1/1 island exists even without $\tilde{b}$. The natural island remains existing even at the operating field B_0=0.9 T, and this will be discussed elsewhere in detail. The poloidal phase of the natural island happens to be almost the same as that of the externally generated island. Thus the obtained configuration can be used for the LID experiment, although the divertor head was designed for the ideal island configuration without error fields. It was shown that there is an inherently high flexibility of the island configuration. By varying $\iota/2\pi$, vertical field or the perturbation coil current I_{pert}, both the island size and position can be modified. In our experiment, however, the standard island configuration was mainly used, whose external condition for the island configuration was utilized for the design of the divertor head.

We found that the plasma parameters change significantly when the island is formed. The line-averaged electron density n_e and the OV radiation intensity decrease significantly with $\tilde{b}$ on, as shown in Figs. 3(a) and 3(b), where a comparison between discharges with $\tilde{b}$ on and off is made at a fixed level of gas puffing. Figure 3 depicts temporal evolutions of n_e, the OV radiation intensity and the stored energy W_{dia} with and without $\tilde{b}$. The stored energy W_{dia}, measured by a diamagnetic loop, also decreases with $\tilde{b}$ on, but its reduction rate is much smaller than that of n_e, because T_e increases, as shown in Fig. 4(a). Figure 4(a) depicts the radial T_e profiles with and without $\tilde{b}$ after the gas puffing, observed by a YAG Thomson scattering system. On the basis of these data, the temporal evolution of the energy confinement time τ_E is estimated. Figure 4(b) depicts the energy confinement time τ_E normalized by that of the LHD scaling law, $\tau_{LHD}=0.17a^{2.0}R_m^{0.75}B_0^{0.84}n_e^{0.69}P_{tot}^{-0.58}$, where a, R_m, and P_{tot} are the averaged plasma radius, the major radius and the total absorbed power, respectively. We found that τ_E/τ_{LHD} with $\tilde{b}$ on is greater than unity and that without $\tilde{b}$, especially after the gas puffing. There is a little uncertainty in estimating P_{tot} with $\tilde{b}$ on because of

lower n_e. To avoid this uncertainty, we compare W_{dia} with and without $\tilde{b}$ at the fixed level of n_e. We found that W_{dia} in the discharge with $\tilde{b}$ on is about 20% higher than that without $\tilde{b}$. These experimental evidences confirm surely that the energy confinement is improved with $\tilde{b}$ on.

An IR TV camera was used to measure the temperature profile of the target surface, and it was found that the position of the maximum temperature rise changes as the position of the divertor head is changed. The position of the maximum temperature rise is situated about 1 cm away from the leading edges when the leading edges are well inside the island. This indicates that the outward heat flux from the core is guided to the back side of the divertor head along the island separatrix. Thus there will be no leading-edge problem in the LID configuration even if the input power is increased significantly. The maximum temperature rise on the target plates during the discharge was observed to be about 5^{O}C.

The neutral particle pressure P_0 in the pumping duct was measured with an fast-ion gauge [7] located just behind the divertor head. The pressure P_0 with a divertor head position r_h=0 cm is shown in Fig. 5(a). Here the axis r_h is R_{hs}-R_h where R_h is the major radial location of the divertor head and R_{hs} is that optimized in the design phase. When $\tilde{b}$ is turned on, P_0 becomes a factor of 1.5 - 2 higher than that without $\tilde{b}$ despite lower core density with $\tilde{b}$ on, as shown in Fig. 5(a). The ion saturation current J_{is} is also shown in Fig. 5(b), which was measured with the Langmuir probe located behind the divertor head. It is clear that J_{is} with $\tilde{b}$ on is a factor of 1.5 - 2 larger than that without $\tilde{b}$, and this is consistent with the fast-ion gauge result. It should be noted that J_{is} without $\tilde{b}$ is almost kept constant even after the gas puff is turned off, while J_{is} with $\tilde{b}$ on decreases rapidly after the gas puffing. This suggests that efficient pumping of the recycled neutral particles takes place by the LID. On the basis of the particle flux calculated using J_{is} behind the divertor head, the pumping rate of the LID is roughly estimated to be in the range from a few percent to about 10%. The radial T_e profiles behind the divertor head were also measured with the Langmuir probe. The temperature

T_e during the gas puffing with $\tilde{b}$ on is higher than that without $\tilde{b}$ by a factor of 2, and T_e after the gas puffing is also higher by a factor of 3 near the leading edge, whereas J_{is} is lower than that without $\tilde{b}$.

The dependence of P_0 and n_e on the island configuration was investigated by changing I_{pert} and at a fixed position of the divertor head, as shown in Fig. 6(a). The size of the island was confirmed to change with I_{pert} by the mapping, mentioned above. The position of the island O-point is not affected by I_{pert}. When I_{pert} is gradually increased from 0 kA, P_0 increases abruptly at about 0.3 kA and is kept almost constant or decreases gradually until about 0.9 kA. Further increase in I_{pert} leads to the abrupt decrease in P_0. The pressure P_0 at I_{pert}=1.1 kA is almost equal to that at I_{pert}=0 kA. The pressure P_0 normalized by n_e has a clear peak at about 0.65 kA. On the other hand, n_e decreases gradually when I_{pert} is increased from 0 kA, and has a minimum at about 0.65 kA, corresponding to the value of I_{pert} for the maximum of P_0/n_e. It is an experimental demonstration that the LID function is sensitive to the LID geometry (island size, position and shape of the head). When it is optimized, the pumping efficiency is maximized, evidenced by the maximum P_0/n_e, leading to the minimum n_e. The standard island configuration corresponds to that with I_{pert}=0.6 kA.

To clarify the I_{pert} dependence of P_0, the plasma behind the divertor head was studied in detail with fixed Langmuir probes, which are mounted directly on the divertor head. The fixed probes are located radially 1 cm away from the leading edges of the divertor head. The radial J_{is} profiles at t=0.08 sec during the gas puffing with and without $\tilde{b}$ are shown in Fig. 6(b), which were measured by changing the head position r_h, so the horizontal axis is the radial position r_h of the divertor head. The ion saturation current J_{is} without $\tilde{b}$ increases monotonically with r_h. When $\tilde{b}$ is turned on, J_{is} becomes larger for r_h< 0 cm, and J_{is} at r_h=1 cm becomes smaller than that at r_h=0 cm, as shown in Fig. 6(b). The peak of the profile at r_h=0 cm corresponds to the outer island separatrix. Lower J_{is} at r_h=1 cm means that the plasma density just inside the outer separatrix is lower than that at the outer separatrix, because part of the divertor head is

located inside the separatrix. As I_{pert} and hence the size of the island are increased, the peak position in the radial J_{is} profile moves towards the outside. The gap between the divertor head and pumping duct is fixed spatially, through which the edge plasma enters the pumping duct, and hence, the change in the peak position of the J_{is} profile explains well the I_{pert} dependence of P_0, shown in Fig. 6(a).

A CCD TV camera with an optical filter was used to measure the Hα radiation intensity near the target plates. The CCD TV camera is set behind the divertor head, as shown in Fig. 2, since the edge plasma enters the pumping duct and strikes the target plates. We found that the Hα radiation intensity behind the divertor head is higher with $\tilde{b}$ on than without $\tilde{b}$. The Hα radiation intensity behind the divertor head behaves similarly as P_0 in the pumping duct.

The edge plasma behavior with and without $\tilde{b}$ was measured with Langmuir probes and a thermal lithium beam probe [9], depicted in Fig. 2. Figure 7 shows the radial profiles of the electron density with and without $\tilde{b}$, measured with the lithium beam probe. The density profiles depicted in Fig. 7(a) were measured at t=0.09 sec during the gas puffing, while the profiles in Fig. 7(b) were obtained at t=0.11 sec after the gas puffing. The edge density with $\tilde{b}$ on is found to decrease a little during the gas puffing compared with that without $\tilde{b}$, and to decrease significantly after the gas puff is turned off. The J_{is} profiles, obtained with the Langmuir probes, are very similar [8]. The Langmuir probe measurement also yields the electron temperature T_e, which is higher when $\tilde{b}$ is turned on than that without $\tilde{b}$, especially just after the gas puff is turned off and before the edge density becomes too low. This is consistent with the result obtained with the Langmuir probe behind the divertor head. The high-temperature and low-density edge plasma realized somewhat in our experiment suggests the feasibility of a low recycling operational mode in LHD that could lead to a significant energy confinement improvement [2]. The low recycling mode of operation will be pursued in the LHD experiment, combined with highly efficient pump and core fueling. The lithium beam probe was also used to measure the broadband density fluctuations in the

edge region, and a correlation dimension and the largest Lyapunov exponent [10] were obtained. Aims of this study are understanding of an effect of chaos on particle transport, which could be helpful in realizing a substantial improvement of the energy confinement in the LHD experiment.

4. SUMMARY

The fundamental functions of the LID have been clearly demonstrated in the present experiment. The leading edges of the divertor head, located inside the island, are protected from the outward heat flux from the core. The particle flow is indeed guided to the back side of the divertor head by the island magnetic field structure, and a high pumping efficiency can be realized even in CHS to some extent. A much higher pumping rate will be achieved in LHD, because a majority of plasma flux flowing outwards is expected to be guided to the target plates on the divertor head without diffusing to the wall due to LHD's smaller diffusion coefficient and larger size. The LID has been also found to affect the core plasma parameters significantly, especially to improve the energy confinement.

We have not yet completed the experimental analysis, but the results analyzed so far are very encouraging in terms of effectiveness of the LID. The LID experiment has provided us critical information on the edge plasma behavior, and helped us to optimize the design of the LID and the closed full helical divertor on LHD.

REFERENCES

[1] IIYOSHI, A., et al., Fusion Technol. **17** (1990) 169.

[2] OHYABU, N., et al., Nucl. Fusion **34** (1994) 387.

[3] KOMORI, A., et al., in Plasma Physics and Controlled Nuclear Fusion Research 1994 (Proc. 15th Int. Conf. Seville, 1994), vol. 2, p. 773.

[4] SARDEI, F., et al., J. Nucl. Mater. (to be published).

[5] GRIEGER, G., et al., in Plasma Physics and Controlled Nuclear Fusion Research 1990 (Proc. 13th Int. Conf. Washington, DC, 1990), vol. 3, p. 525.

[6] MATSUOKA, K., et al., in Plasma Physics and Controlled Nuclear Fusion Research 1988 (Proc. 12th Int. Conf. Nice, 1988), vol. 2, p. 411.

[7] HAAS, G., et al., J. Nucl. Mater. **121** (1984) 151.

[8] KOMORI, A., et al., J. Nucl. Mater. (to be published).

[9] KOMORI, A., et al., Nucl. Fusion **28** (1988) 1460.

[10] KOMORI, A., et al., Phys. Rev. Lett. **73** (1994) 660.

FIGURE CAPTIONS

Fig. 1. Local island divertor concept. (a) LID configuration and particle flow to target plates. (b) Schematic view explaining the relation between divertor head and island separatrix.

Fig. 2. Schematic view of experimental apparatus.

Fig. 3. Comparison of temporal evolutions of (a) averaged electron density n_e, (b) OV radiation intensity and (c) stored energy W_{dia} between two discharges with and without $\tilde{b}$.

Fig. 4. (a) Radial T_e profiles with and without $\tilde{b}$, measured at t=0.1085 sec after the gas puffing. (b) Energy confinement time τ_E normalized by that of the LHD scaling law τ_{LHD}. In the upper figure, R is a radial position from the major axis.

Fig. 5. Comparison of temporal evolutions of (a) neutral hydrogen pressure P_0 and (b) ion saturation current J_{is} behind the divertor head between two discharges with and without $\tilde{b}$.

Fig. 6. Dependence of edge plasma parameters on LID geometry. (a) Dependence of P_0, n_e and P_0/n_e on the perturbation coil current I_{pert}. (b) Radial J_{is} profiles with and without $\tilde{b}$ at t=0.08 sec during the gas puffing, measured with a Langmuir probe fixed on the divertor head.

Fig. 7. Electron density profiles with and without $\tilde{b}$, measured with a thermal lithium beam probe. (a) Profiles during the gas puffing. (b) Profiles after the gas puffing. The r_{Li} axis points toward the wall, and the separatrix is located at r_{Li}~14.3 cm.

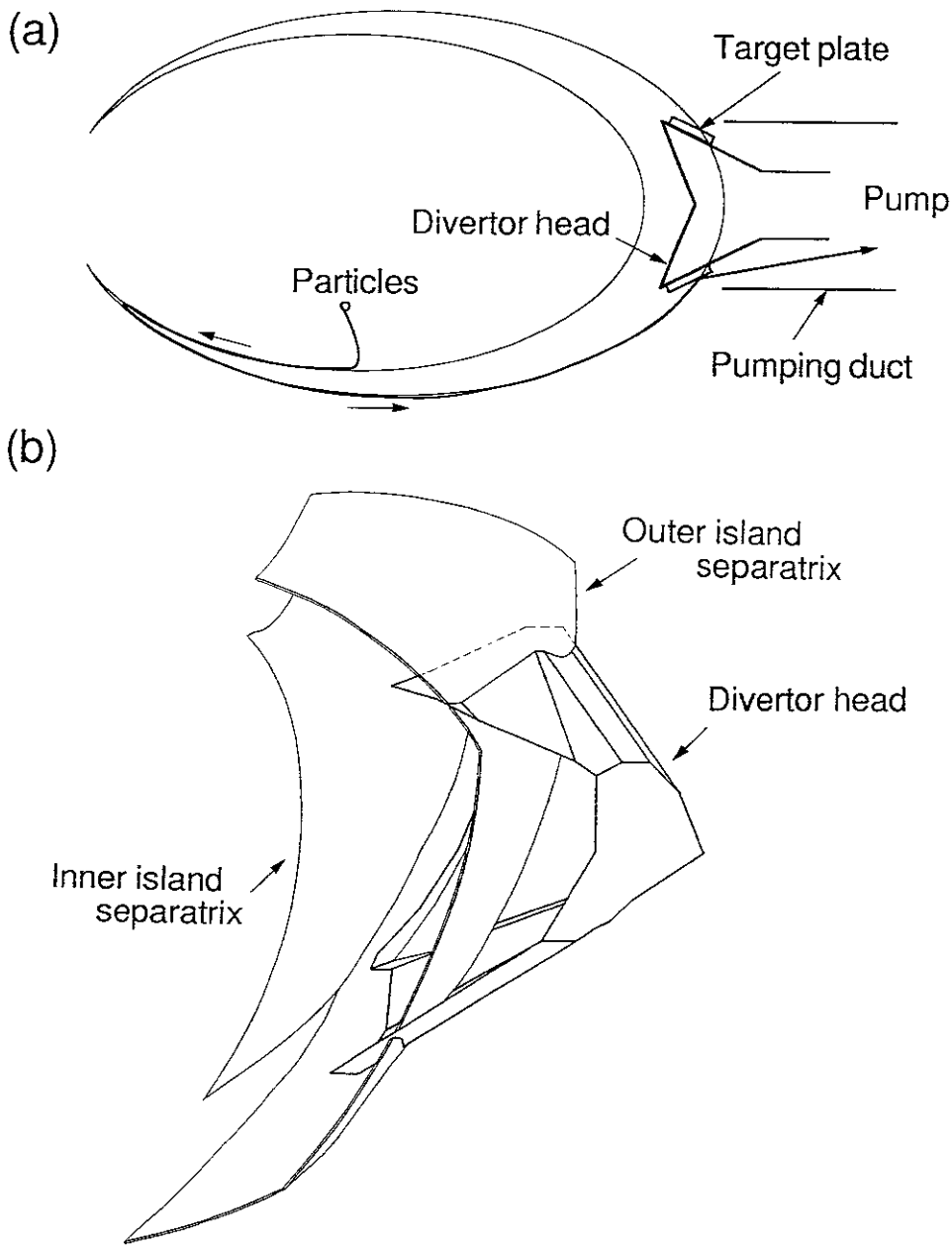
(a)
Target plate
Pump
Divertor head
Particles
Pumping duct
(b)
Outer island
separatrix
Divertor head
Inner island
separatrix

Fig. 1

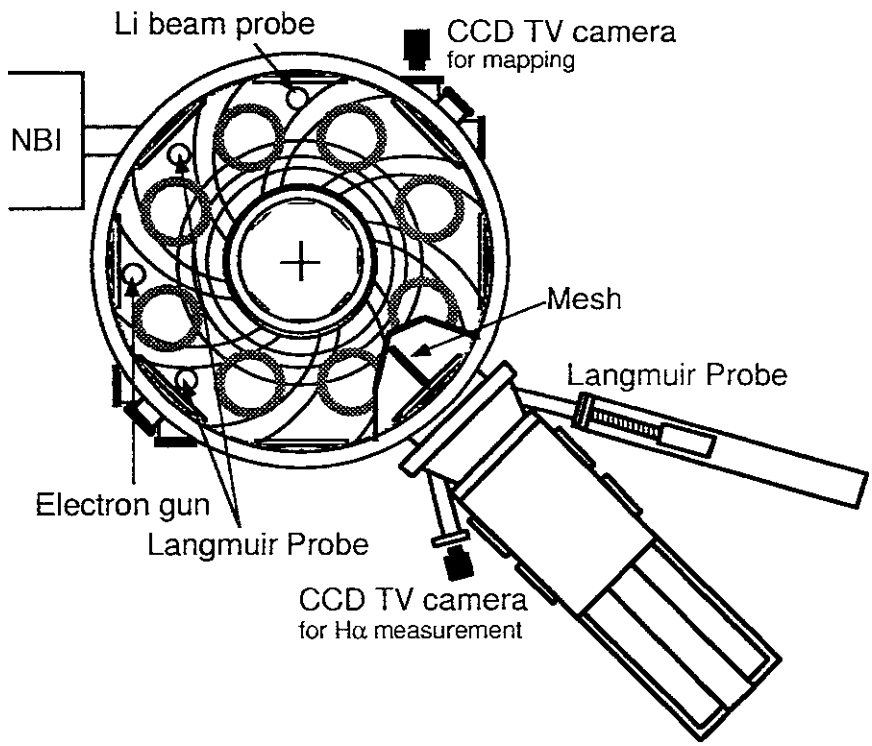
Li beam probe
CCD TV camera
for mapping
NBI
Mesh
Langmuir Probe
Electron gun
Langmuir Probe
CCD TV camera
for Hα measurement

Fig. 2

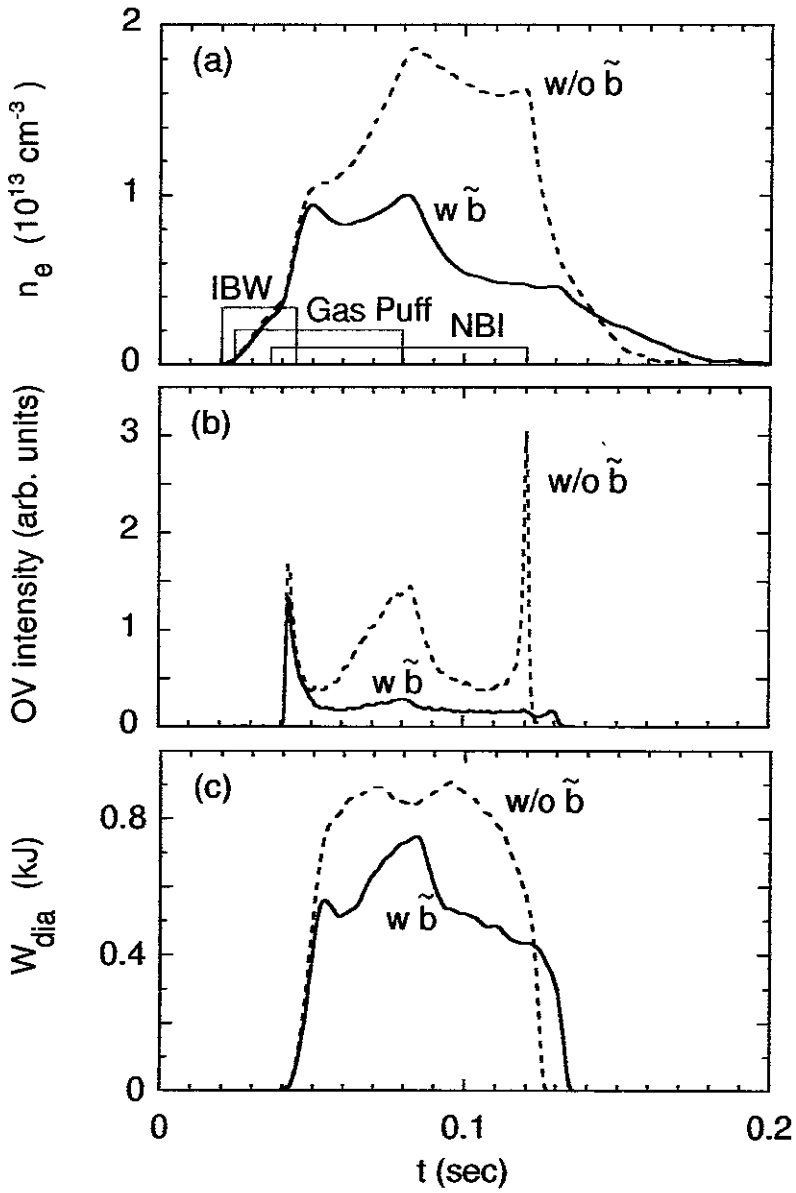
(a)
w/o $\tilde{b}$
w $\tilde{b}$
IBW
Gas Puff
NBI
n_e (10^{13} cm^{-3})
(b)
w/o $\tilde{b}$
w $\tilde{b}$
OV intensity (arb. units)
(c)
w/o $\tilde{b}$
w $\tilde{b}$
W_{dia} (kJ)
t (sec)

Fig. 3

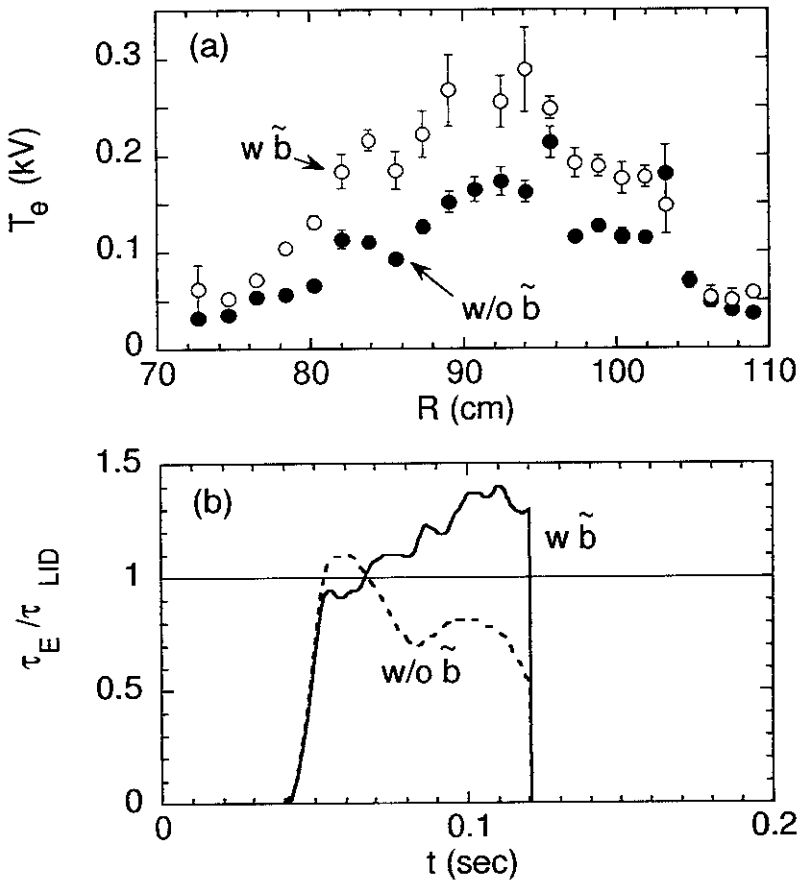
(a)
w $\tilde{b}$
w/o $\tilde{b}$
T_e (kV)
0.3
0.2
0.1
0
70
80
90
100
110
R (cm)
(b)
w $\tilde{b}$
w/o $\tilde{b}$
τ_E/τ_{LID}
1.5
1
0.5
0
0
0.1
0.2
t (sec)

Fig. 4

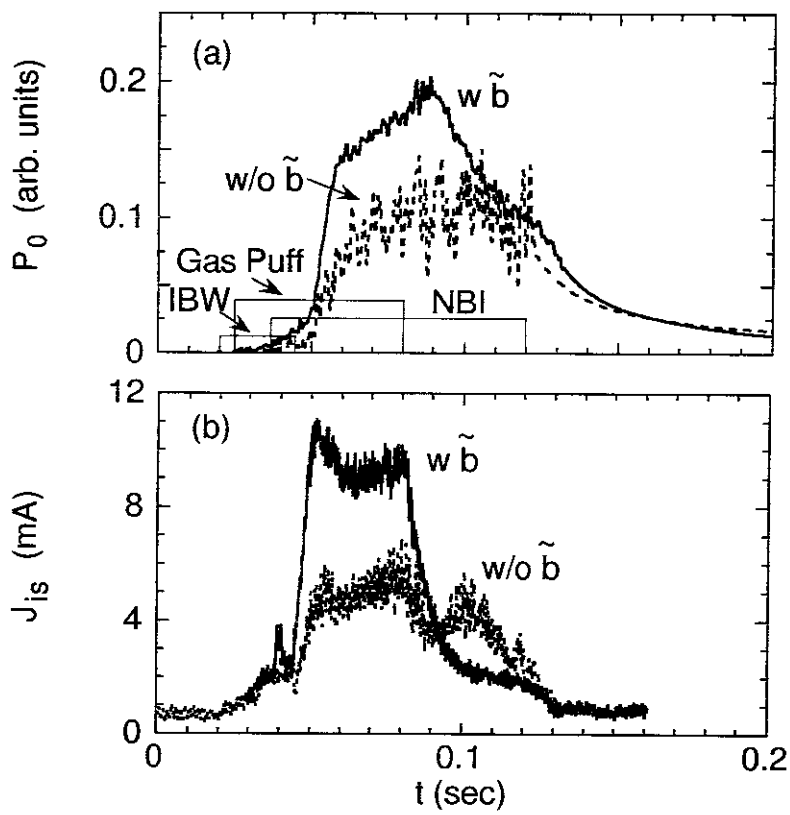
(a)
0.2
0.1
0
P_0 (arb. units)
w $\tilde{b}$
w/o $\tilde{b}$
Gas Puff
IBW
NBI
12
8
4
0
(b)
J_{is} (mA)
w $\tilde{b}$
w/o $\tilde{b}$
0
0.1
0.2
t (sec)

Fig. 5

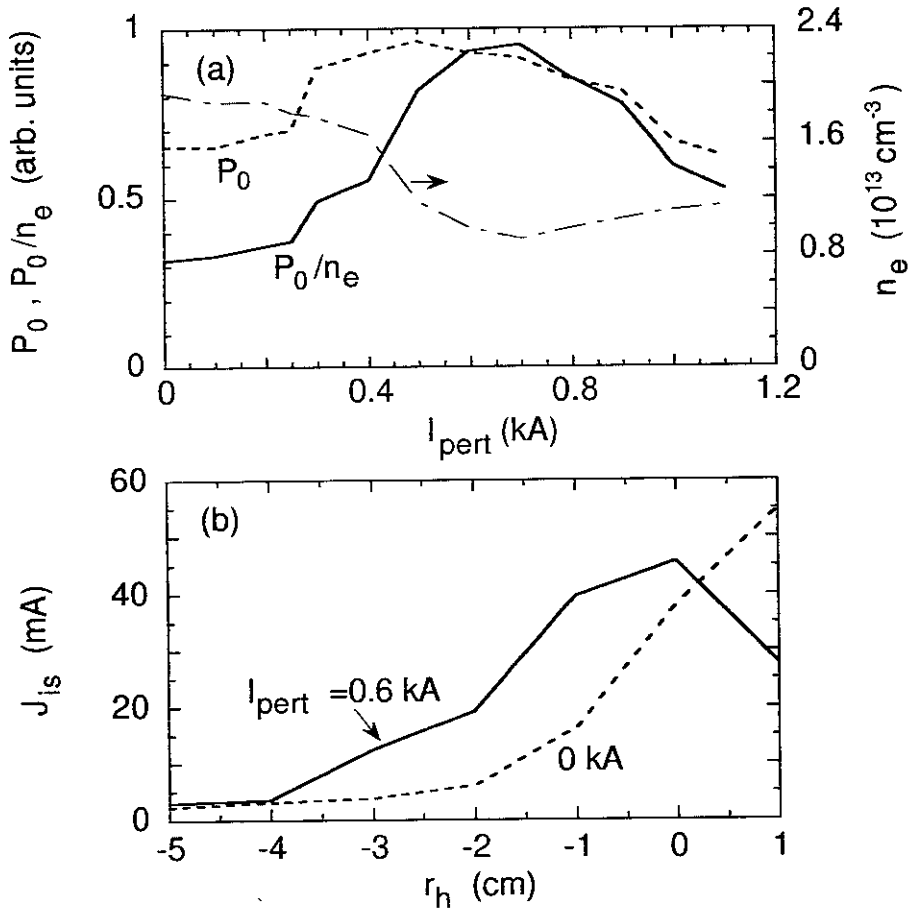
(a)
P_0
P_0/n_e
P_0 , P_0/n_e (arb. units)
n_e (10^{13} cm^{-3})
I_{pert} (kA)
(b)
I_{pert} =0.6 kA
0 kA
J_{is} (mA)
r_h (cm)

Fig. 6

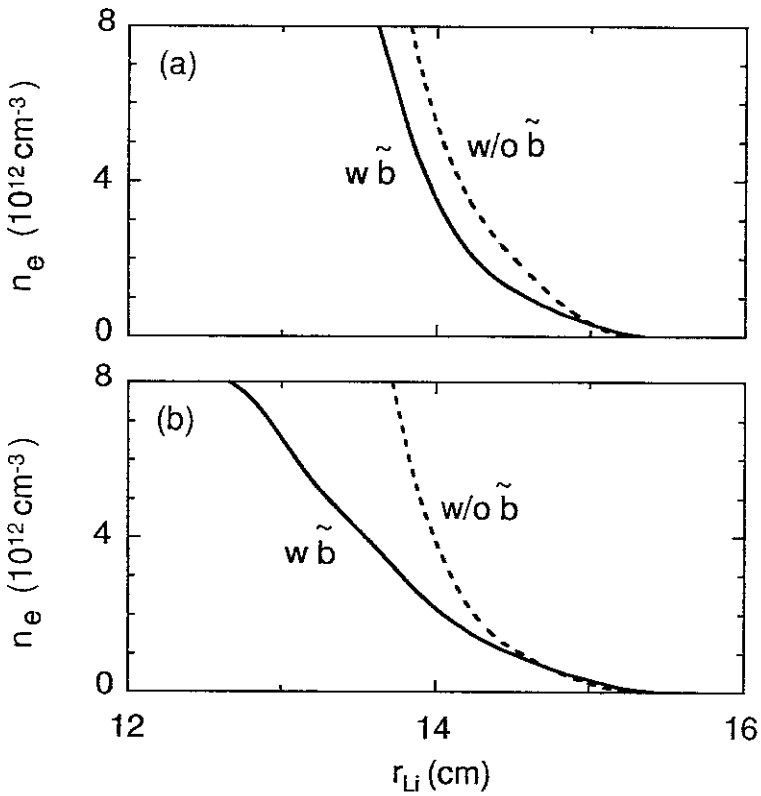

Fig. 7

Recent Issues of NIFS Series

NIFS-395 H. Sugama and M. Okamoto, W. Horton and M. Wakatani.
Transport Processes and Entropy Production in Toroidal Plasmas with Gyrokinetic Eletromagnetic Turbulence: Jan. 1996

NIFS-396 T. Kato, T. Fujiwara and Y. Hanaoka,
X-ray Spectral Analysis of Yohkoh BCS Data on Sep. 6 1992 Flares - Blue Shift Component and Ion Abundances -; Feb. 1996

NIFS-397 H. Kuramoto, N. Hiraki, S. Moriyama, K. Toi, K. Sato, K. Narihara, A. Ejiri, T. Seki and JIPP T-IIU Group,
Measurement of the Poloidal Magnetic Field Profile with High Time Resolution Zeeman Polarimeter in the JIPP T-IIU Tokamak; Feb. 1996

NIFS-398 J.F. Wang, T. Amano, Y. Ogawa, N. Inoue,
Simulation of Burning Plasma Dynamics in ITER; Feb. 1996

NIFS-399 K. Itoh, S-I. Itoh, A. Fukuyama and M. Yagi,
Theory of Self-Sustained Turbulence in Confined Plasmas; Feb. 1996

NIFS-400 J. Uramoto,
A Detection Method of Negative Pionlike Particles from a H2 Gas Descharge Plasma; Feb. 1996

NIFS-401 K.Ida, J.Xu, K.N.Sato, H.Sakakita and JIPP TII-U group,
Fast Charge Exchange Spectroscopy Using a Fabry-Perot Spectrometer in the JIPP TII-U Tokamak; Feb. 1996

NIFS-402 T. Amano,
Passive Shut-Down of ITER Plasma by Be Evaporation; Feb. 1996

NIFS-403 K. Orito,
A New Variable Transformation Technique for the Nonlinear Drift Vortex; Feb. 1996

NIFS-404 T. Oike, K. Kitachi, S. Ohdachi, K. Toi, S. Sakakibara, S. Morita, T. Morisaki, H. Suzuki, S. Okamura, K. Matsuoka and CHS group; *Measurement of Magnetic Field Fluctuations near Plasma Edge with Movable Magnetic Probe Array in the CHS Heliotron/Torsatron*; Mar. 1996

NIFS-405 S.K. Guharay, K. Tsumori, M. Hamabe, Y. Takeiri, O. Kaneko, T. Kuroda,
Simple Emittance Measurement of H- Beams from a Large Plasma Source; Mar. 1996

NIFS-406 M. Tanaka and D. Biskamp,
Symmetry-Breaking due to Parallel Electron Motion and Resultant Scaling in Collisionless Magnetic Reconnection; Mar. 1996

NIFS-407 K. Kitachi, T. Oike, S. Ohdachi, K. Toi, R. Akiyama, A. Ejiri, Y. Hamada, H.Kuramoto, K. Narihara, T. Seki and JIPP T-IIU Group,
Measurement of Magnetic Field Fluctuations within Last Closed Flux Surface with Movable Magnetic Probe Array in the JIPP T-IIU Tokamak; Mar. 1996

NIFS-408 K. Hirose, S. Saito and Yoshi.H. Ichikawa
Structure of Period-2 Step-1 Accelerator Island in Area Preserving Maps; Mar. 1996

NIFS-409 G.Y.Yu, M. Okamoto, H. Sanuki, T. Amano,
Effect of Plasma Inertia on Vertical Displacement Instability in Tokamaks; Mar. 1996

NIFS-410 T. Yamagishi,
Solution of Initial Value Problem of Gyro-Kinetic Equation; Mar. 1996

NIFS-411 K. Ida and N. Nakajima,
Comparison of Parallel Viscosity with Neoclassical Theory; Apr. 1996

NIFS-412 T. Ohkawa and H. Ohkawa,
Cuspher, A Combined Confinement System; Apr. 1996

NIFS-413 Y. Nomura, Y.H. Ichikawa and A.T. Filippov,
Stochasticity in the Josephson Map; Apr. 1996

NIFS-414 J. Uramoto,
Production Mechanism of Negative Pionlike Particles in H_2 Gas Discharge Plasma; Apr. 1996

NIFS-415 A. Fujisawa, H. Iguchi, S. Lee, T.P. Crowley, Y. Hamada, S. Hidekuma, M. Kojima,
Active Trajectory Control for a Heavy Ion Beam Probe on the Compact Helical System; May 1996

NIFS-416 M. Iwase, K. Ohkubo, S. Kubo and H. Idei
Band Rejection Filter for Measurement of Electron Cyclotron Emission during Electron Cyclotron Heating; May 1996

NIFS-417 T. Yabe, H. Daido,T. Aoki, E. Matsunaga and K. Arisawa,
Anomalous Crater Formation in Pulsed-Laser-Illuminated Aluminum Slab and Debris Distribution; May 1996

NIFS-418 J. Uramoto,
Extraction of K^- Mesonlike Particles from a D_2 Gas Discharge Plasma in Magnetic Field; May 1996

NIFS-419 J. Xu, K. Toi, H. Kuramoto, A. Nishizawa, J. Fujita, A. Ejiri, K. Narihara, T. Seki, H. Sakakita, K. Kawahata, K. Ida, K. Adachi, R. Akiyama, Y. Hamada, S. Hirokura, Y. Kawasumi, M. Kojima, I. Nomura, S. Ohdachi, K.N. Sato
Measurement of Internal Magnetic Field with Motional Stark Polarimetry in Current Ramp-Up Experiments of JIPP T-IIU; June 1996

NIFS-420 Y.N. Nejoh,
Arbitrary Amplitude Ion-acoustic Waves in a Relativistic Electron-beam Plasma System; July 1996

NIFS-421 K. Kondo, K. Ida, C. Christou, V.Yu.Sergeev, K.V.Khlopenkov, S.Sudo, F. Sano, H. Zushi, T. Mizuuchi, S. Besshou, H. Okada, K. Nagasaki, K. Sakamoto, Y. Kurimoto, H. Funaba, T. Hamada, T. Kinoshita, S. Kado, Y. Kanda, T. Okamoto, M. Wakatani and T. Obiki,
Behavior of Pellet Injected Li Ions into Heliotron E Plasmas; July 1996

NIFS-422 Y. Kondoh, M. Yamaguchi and K. Yokozuka,
Simulations of Toroidal Current Drive without External Magnetic Helicity Injection; July 1996

NIFS-423 Joong-San Koog,
Development of an Imaging VUV Monochromator in Normal Incidence Region: July 1996

NIFS-424 K. Orito,
A New Technique Based on the Transformation of Variables for Nonlinear Drift and Rossby Vortices; July 1996

NIFS-425 A. Fujisawa, H. Iguchi, S. Lee, T.P. Crowley, Y. Hamada, H. Sanuki, K. Itoh, S. Kubo, H. Idei, T. Minami, K. Tanaka, K. Ida, S. Nishimura, S. Hidekuma, M. Kojima, C. Takahashi, S. Okamura and K. Matsuoka,
Direct Observation of Potential Profiles with a 200keV Heavy Ion Beam Probe and Evaluation of Loss Cone Structure in Toroidal Helical Plasmas on the Compact Helical System; July 1996

NIFS-426 H. Kitauchi, K. Araki and S. Kida,
Flow Structure of Thermal Convection in a Rotating Spherical Shell; July 1996

NIFS-427 S. Kida and S. Goto,
Lagrangian Direct-interaction Approximation for Homogeneous Isotropic Turbulence; July 1996

NIFS-428 V.Yu. Sergeev, K.V. Khlopenkov, B.V. Kuteev, S. Sudo, K. Kondo, F. Sano, H. Zushi, H. Okada, S. Besshou, T. Mizuuchi, K. Nagasaki, Y. Kurimoto and T. Obiki,
Recent Experiments on Li Pellet Injection into Heliotron E; Aug. 1996

NIFS-429 N. Noda, V. Philipps and R. Neu,
A Review of Recent Experiments on W and High Z Materials as Plasma-Facing Components in Magnetic Fusion Devices; Aug. 1996

NIFS-430 R.L. Tobler, A. Nishimura and J. Yamamoto,
Design-Relevant Mechanical Properties of 316-Type Stainless Steels for Superconducting Magnets; Aug. 1996

NIFS-431 K. Tsuzuki, M. Natsir, N. Inoue, A. Sagara, N. Noda, O. Motojima, T. Mochizuki, T. Hino and T. Yamashina,
Hydrogen Absorption Behavior into Boron Films by Glow Discharges in Hydrogen and Helium; Aug. 1996

NIFS-432 T.-H. Watanabe, T. Sato and T. Hayashi,
Magnetohydrodynamic Simulation on Co- and Counter-helicity Merging of Spheromaks and Driven Magnetic Reconnection; Aug. 1996

NIFS-433 R. Horiuchi and T. Sato,
Particle Simulation Study of Collisionless Driven Reconnection in a Sheared Magnetic Field; Aug. 1996

NIFS-434 Y. Suzuki, K. Kusano and K. Nishikawa,
Three-Dimensional Simulation Study of the Magnetohydrodynamic Relaxation Process in the Solar Corona. II.; Aug. 1996

NIFS-435 H. Sugama and W. Horton,
Transport Processes and Entropy Production in Toroidally Rotating Plasmas with Electrostatic Turbulence; Aug. 1996

NIFS-436 T. Kato, E. Rachlew-Källne, P. Hörling and K.-D Zastrow,
Observations and Modelling of Line Intensity Ratios of OV Multiplet Lines for 2s3s 3S1 - 2s3p 3Pj; Aug. 1996

NIFS-437 T. Morisaki, A. Komori, R. Akiyama, H. Idei, H. Iguchi, N. Inoue, Y. Kawai, S. Kubo, S. Masuzaki, K. Matsuoka, T. Minami, S. Morita, N. Noda, N. Ohyabu, S. Okamura, M. Osakabe, H. Suzuki, K. Tanaka, C. Takahashi, H. Yamada, I. Yamada and O. Motojima,
Experimental Study of Edge Plasma Structure in Various Discharges on Compact Helical System; Aug. 1996

NIFS-438 A. Komori, N. Ohyabu, S. Masuzaki, T. Morisaki, H. Suzuki, C. Takahashi, S. Sakakibara, K. Watanabe, T. Watanabe, T. Minami, S. Morita, K. Tanaka, S. Ohdachi, S. Kubo, N. Inoue, H. Yamada, K. Nishimura, S. Okamura, K. Matsuoka, O. Motojima, M. Fujiwara, A. Iiyoshi, C. C. Klepper, J.F. Lyon, A.C. England, D.E. Greenwood, D.K. Lee, D.R. Overbey, J.A. Rome, D.E. Schechter and C.T. Wilson,
Edge Plasma Control by a Local Island Divertor in the Compact Helical System; Sep. 1996 (IAEA-CN-64/C1-2)